Simultaneous Boundary and Distributed Feedback Control of the Current Profile in H-mode Discharges on DIII-D [★]

Mark D. Boyer [*] **Justin Barton** [*] **Wenyu Shi** [*]
William Wehner [*] **Eugenio Schuster** [*] **John Ferron** [**]
Mike Walker [**] **Dave Humphreys** [**] **Francesca Turco** [***]
Tim Luce [**] **Robert Johnson** [**] **Benjamin Penaflor** [**]

[*] *Lehigh University, Bethlehem, PA 18015, USA.*
[**] *General Atomics, San Diego, CA 92121, USA.*
[***] *Columbia University, New York, NY 10027, USA.*

Abstract: Control of the current profile in tokamak plasmas has been shown to play an important role in achieving advanced scenarios that could enable steady-state operation. The nonlinearity and spatially distributed nature of the current profile dynamics motivate the use of model-based control designs. In this work, we consider a control-oriented model of the current profile evolution in DIII-D high-confinement (H-mode) discharges, and the problem of regulating the current profile around a desired trajectory. The PDE model is discretized in space with a finite difference method and a backstepping design is applied to obtain a transformation from the original system into a particular target system with desirable properties. The resulting boundary condition control law is complemented with control laws for the available distributed actuators. The combined control strategy uses nonlinear combinations of the total plasma current, total power, and line averaged density as actuators. Simulation and experimental results show the ability of the controller to track desired targets and to reject input disturbances.

1. INTRODUCTION

In nuclear fusion reactions, two light nuclei fuse together to form a heavier nucleus, resulting in conversion of mass into energy. To produce useful levels of power, fusion reactors must reach extremely high temperatures. At these temperatures, the deuterium/tritium fuel mixture becomes a plasma. One of the most promising devices for confining fusion plasmas is the tokamak, which uses helical magnetic fields to trap fuel particles. The ITER tokamak, the next experimental step for fusion research, will attempt to show the technical feasibility of a fusion power plant.

One of the challenges in fusion is to operate the tokamak with sufficiently long discharges. Steady-state operation will require the plasma current, needed for a stable magnetic equilibrium, to be entirely driven by non-inductive means. It has been shown that setting up a suitable toroidal current profile plays an important role in non-inductive plasma current sustainment (see Murakami et al. (2006)), motivating work on current profile control at many devices, including JET (Laborde et al., 2005; Moreau et al., 2008), Tore Supra, and JT-60U (Wijnands et al., 1997; Barana et al., 2007; Suzuki et al., 2008), as well as DIII-D, the subject of this work.

The current profile evolution is related to the evolution of the poloidal magnetic flux, which can be modeled in cylindrical coordinates by a parabolic partial differential equation (PDE) referred to as the magnetic diffusion equation. The poloidal flux profile is related to the safety factor q, the ratio of the number of times a magnetic field line goes around the tokamak toroidally to the number of times it goes around poloidally. Non-model-based active control of the safety factor at the magnetic axis, $q(0)$, and the minimum safety factor q_{min} during the initial part of the plasma discharge has been tested at DIII-D (Ferron et al., 2006). However, limitations, such as oscillations and instability under certain conditions, along with the complexity and nonlinearity of the multi-input-multi-output system, motivate the design of model-based controllers that take the dynamic response of the q profile into account.

A first-principles-driven control-oriented model of the current profile evolution in L-mode (low confinement) discharges in DIII-D was developed in Ou et al. (2007). The bootstrap current, a self-generated, non-inductive current source, was neglected, since this effect is small in L-mode discharges. The L-mode model was used to generate optimal feedforward actuator trajectories (Ou et al., 2008; Xu et al., 2010), and to design feedback controllers that were tested experimentally in Barton et al. (2012); Boyer et al. (2013, 2014). In this work, an extension of the model that includes the bootstrap current and is therefore suitable for H-mode (high confinement) discharges is used to develop a
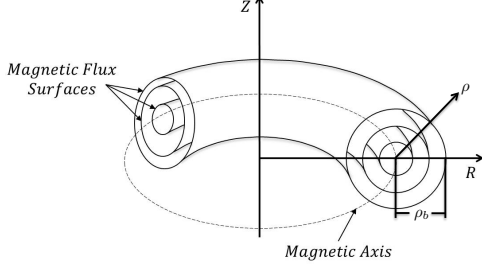
Fig. 1. Coordinates used in current profile model.

model-based controller (details of the model development can be found in Barton et al. (2013)). The PDE describing the current profile evolution is discretized in space using a finite difference method and a backstepping technique is applied to obtain a transformation from the original system into a particular target system. The transformation is used to find a boundary condition control law, which is then complemented with control laws for the available distributed actuators through Lyapunov analysis of the target system. Numerical simulations show the ability of the scheme to track target profiles, and the disturbance rejection capability of the scheme is shown in a preliminary experiment on DIII-D. The paper is organized as follows. In Section 2 the current profile model is given. The control objective and design are presented in Section 3. Simulation and experimental results are discussed in Section 4. Conclusions are stated in Section 5.

2. CURRENT PROFILE EVOLUTION MODEL

Figure 1 depicts the coordinate system used in this work. To index the magnetic surfaces within a poloidal cross-section of the plasma, we use the mean effective radius of the magnetic surface, denoted as ρ and defined by $\pi B_{\phi,0}\rho^2 = \Phi$, where Φ is the toroidal magnetic flux and $B_{\phi,0}$ is the toroidal magnetic field at the geometric major radius R_0 of the tokamak. We normalize this variable by ρ_b, the mean effective minor radius of the last closed magnetic surface, to obtain the coordinate $\hat{\rho} = \rho/\rho_b$. The safety factor is given by $q(\rho,t) = -\partial\Phi/\partial\Psi(\rho,t)$, where Ψ is the poloidal magnetic flux. This can be written as

$$q(\hat{\rho},t) = -\frac{B_{\phi,0}\rho_b^2\hat{\rho}}{\partial\psi/\partial\hat{\rho}}, \qquad (1)$$

where ψ represents the poloidal stream function ($\Psi = 2\pi\psi$), by noting $\pi B_{\phi,0}\rho^2 = \Phi$ and the definition of ρ_b. Since the safety factor depends inversely on the spatial derivative of the poloidal flux, we take as the variable of interest

$$\theta(\hat{\rho},t) = \frac{\partial\psi}{\partial\hat{\rho}}(\hat{\rho},t). \qquad (2)$$

To obtain a PDE for $\theta(\hat{\rho},t)$, we start from the magnetic diffusion equation (Hinton and Hazeltine, 1976), given by

$$\frac{\partial\psi}{\partial t} = \frac{\eta(T_e)}{\mu_0\rho_b^2\hat{F}^2}\frac{1}{\hat{\rho}}\frac{\partial}{\partial\hat{\rho}}\left(\hat{\rho}\hat{F}\hat{G}\hat{H}\frac{\partial\psi}{\partial\hat{\rho}}\right)$$
$$+ R_0\hat{H}\eta(T_e)\frac{<\bar{j}_{NI}\cdot\bar{B}>}{B_{\phi,0}}, \qquad (3)$$

where t is time, η is the resistivity, which is dependent on the electron temperature, T_e, μ_0 is the vacuum permeability, $\bar{j}_{NI}$ is the non-inductive current density, $\bar{B}$ is

the toroidal magnetic field, and $<>$ denotes the flux-surface average of a quantity. $\hat{F}$, $\hat{G}$, and $\hat{H}$ are spatially varying geometric factors of the DIII-D tokamak described in Barton et al. (2013). The boundary conditions are

$$\frac{\partial\psi}{\partial\hat{\rho}}\bigg|_{\hat{\rho}=0} = 0, \quad \frac{\partial\psi}{\partial\hat{\rho}}\bigg|_{\hat{\rho}=1} = -\frac{\mu_0}{2\pi}\frac{R_0}{\hat{G}|_{\hat{\rho}=1}\hat{H}|_{\hat{\rho}=1}}I(t), \quad (4)$$

where $I(t)$ is the total plasma current.

In order to arrive at a control-oriented model of the current profile evolution, simplified empirical models of plasma parameters are used to capture the dominant physics describing how the available actuators affect the system. The model for the electron density is given by

$$n_e(\hat{\rho},t) = n_e^{prof}(\hat{\rho})\bar{n}(t), \qquad (5)$$

where $n_e^{prof}(\hat{\rho})$ is a reference profile and $\bar{n}(t)$ is the line averaged density. The electron temperature is modeled as

$$T_e(\hat{\rho},t) = k_{T_e}T_e^{profile}(\hat{\rho})I(t)\sqrt{P_{tot}(t)}\bar{n}^{-1}(t), \qquad (6)$$

where k_{T_e} is a constant, $T_e^{profile}(\hat{\rho})$ is a reference profile, $P_{tot}(t)$ is the total NBI and gyrotron heating power. The model for the non-inductive toroidal current density driven by each auxiliary source is given by

$$\frac{<\bar{j}_k\cdot\bar{B}>}{B_{\phi,0}} = k_k j_k^{profile}(\hat{\rho})\frac{T_e(\hat{\rho},t)P_k(t)}{n_e(\hat{\rho},t)}, \qquad (7)$$

where k_k is a constant and $j_k^{profile}(\hat{\rho})$ is a reference profile for the non-inductive current deposition of the k-th auxiliary source. We consider the total gyrotron power ($k = 2$), the total on-axis beam power ($k = 3$), and the total off-axis beam power ($k = 4$) as available sources. The bootstrap current, a self-generated non-inductive current source that arises due to gradients in the magnetic field strength and plasma pressure, is modeled as (Sauter et al., 1999)

$$\frac{<\bar{j}_{bs}\cdot\bar{B}>}{B_{\phi,0}} = \frac{k_{JkeV}R_0}{\hat{F}}\frac{1}{\theta}\left[2\mathcal{L}_{31}T_e\frac{\partial n_e}{\partial\hat{\rho}}\right.$$
$$\left. + \{2\mathcal{L}_{31} + \mathcal{L}_{32} + \alpha\mathcal{L}_{34}\}n_e\frac{\partial T_e}{\partial\hat{\rho}}\right], \qquad (8)$$

where $k_{JkeV} = 1.602 \times 10^{-16}J/keV$, and $\mathcal{L}_{31}(\hat{\rho})$, $\mathcal{L}_{32}(\hat{\rho})$, $\mathcal{L}_{34}(\hat{\rho})$, and $\alpha(\hat{\rho})$ depend on the particular magnetic equilibrium and on the particle collisionality of the plasma. The plasma resistivity, $\eta(T_e)$, is given by

$$\eta(\hat{\rho},t) = k_{eff}Z_{eff}T_e^{-3/2}(\hat{\rho},t), \qquad (9)$$

where k_{eff} is a constant and the effective atomic number Z_{eff} is considered constant.

To obtain a PDE governing the evolution of $\theta(\hat{\rho},t)$, the empirical scaling models for the temperature, resistivity, and current drive are substituted in (3), the result is expanded with the chain rule and differentiated, yielding

$$\frac{\partial\theta}{\partial t} = \left(h_{1a}\frac{\partial^2\theta}{\partial\hat{\rho}^2} + h_{1b}\frac{\partial\theta}{\partial\hat{\rho}} + h_{1c}\theta\right)u_1(t) + \sum_{k=2}^{4}h_k u_k(t)$$
$$+ \left(\frac{1}{\theta}\frac{df_5}{d\hat{\rho}} + \frac{f_5}{\theta^2}\frac{\partial\theta}{\partial\hat{\rho}}\right)u_5(t), \qquad (10)$$

$$\theta(0,t) = 0, \quad \theta(1,t) = -k_6 u_6(t), \qquad (11)$$

where h_{1a}, h_{1b}, h_{1c}, h_k (for $k = 2, 3, 4$), f_5, and D_ψ are functions of $\hat{\rho}$, k_6 is a constant, and

$$u_1(t) = \left(\frac{\bar{n}}{I\sqrt{P_{tot}}}\right)^{3/2}, \ u_k(t) = \frac{P_k}{\left(I\sqrt{P_{tot}}\right)^{1/2}\bar{n}^{1/2}},$$

$$u_5(t) = \frac{\bar{n}^{3/2}}{\left(I\sqrt{P_{tot}}\right)^{1/2}}, \quad u_6(t) = I, \tag{12}$$

for $k = 2, 3, 4$. Equation (10) admits actuators $u = [u_1, \ldots, u_6]$, which each represent nonlinear combinations of the physical actuators, $I(t)$, $\bar{n}(t)$, and $P_k(t)$ for $k = 2, 3, 4$. The controller proposed in this work generates waveforms for these physical actuators. These waveforms represent references to be sent to existing dedicated controllers for each of the respective quantities.

3. CONTROL DESIGN

Let $u_{ff}(t) = \left[u_{1_{ff}}(t), \ldots, u_{6_{ff}}(t)\right]$ represent feedforward control input trajectories and $\theta_{ff}(\hat{\rho}, t)$ be the associated poloidal flux gradient profile evolution for a nominal initial condition $\theta_{ff}(\hat{\rho}, 0)$. The nominal profile satisfies

$$\frac{\partial \theta_{ff}}{\partial t} = \left(h_{1a}\frac{\partial^2 \theta_{ff}}{\partial \hat{\rho}^2} + h_{1b}\frac{\partial \theta_{ff}}{\partial \hat{\rho}} + h_{1c}\theta_{ff}\right)u_{1_{ff}}(t)$$
$$+ \sum_{k=2}^{4} h_k u_{k_{ff}}(t) + g\left(\theta_{ff}\right)u_{5_{ff}}(t),$$
$$\theta_{ff}(0,t) = 0, \quad \theta_{ff}(1,t) = -k_6 u_{6_{ff}}(t),$$

where $g(\theta) = \left(\frac{1}{\theta}\frac{df_5}{d\hat{\rho}} + \frac{f_5}{\theta^2}\frac{\partial \theta}{\partial \hat{\rho}}\right)$. Due to initial condition errors or disturbances, the actual state will differ from the nominal profile, i.e. $\theta(\hat{\rho}, t) = \theta_{ff}(\hat{\rho}, t) + \tilde{\theta}(\hat{\rho}, t)$, where $\tilde{\theta}$ represents the error between the achieved and nominal profile. We consider $u = u_{ff} + u_{fb} + d$ where the feedback control signals $u_{fb}(t) = \left[u_{1_{fb}}(t), \ldots, u_{6_{fb}}(t)\right]$ are generated by to-be-designed control laws and $d = [d_1, \ldots, d_6]$ is a set of constant input disturbances. The error is then given by

$$\frac{\partial \tilde{\theta}}{\partial t} = \left(h_{1a}\frac{\partial^2 \tilde{\theta}}{\partial \hat{\rho}^2} + h_{1b}\frac{\partial \tilde{\theta}}{\partial \hat{\rho}} + h_{1c}\tilde{\theta}\right)u_{1_{ff}} + \tilde{g}u_{5_{ff}}$$
$$+ \left(h_{1a}\frac{\partial^2 \theta}{\partial \hat{\rho}^2} + h_{1b}\frac{\partial \theta}{\partial \hat{\rho}} + h_{1c}\theta\right)\left(u_{1_{fb}} + d_1\right)$$
$$+ \sum_{k=2}^{4} h_k\left(u_{k_{fb}} + d_k\right) + g\left(u_{5_{fb}} + d_5\right), \tag{13}$$
$$\tilde{\theta}(0,t) = 0, \quad \tilde{\theta}(1,t) = -k_6\left(u_{6_{fb}} + d_6\right), \tag{14}$$

where $\tilde{g} = g(\theta) - g(\theta_{ff})$.

We attempt to cancel the unknown disturbances by defining the feedback laws $u_{k_{fb}} = v_k - \hat{d}_k$, for $k = 1, \ldots, 6$, where $\hat{d}_k$ is an estimate of the disturbances, and v_k is a to-be-designed control signal, resulting in

$$\frac{\partial \tilde{\theta}}{\partial t} = \left(h_{1a}\frac{\partial^2 \tilde{\theta}}{\partial \hat{\rho}^2} + h_{1b}\frac{\partial \tilde{\theta}}{\partial \hat{\rho}} + h_{1c}\tilde{\theta}\right)u_{1_{ff}}$$
$$+ \left(h_{1a}\frac{\partial^2 \theta}{\partial \hat{\rho}^2} + h_{1b}\frac{\partial \theta}{\partial \hat{\rho}} + h_{1c}\theta\right)\left(v_1 + \tilde{d}_1\right)$$
$$+ \sum_{k=2}^{4} h_k\left(v_k + \tilde{d}_k\right) + g\left(v_5 + \tilde{d}_5\right) + \hat{g}u_{5_{ff}}\tilde{\theta},$$
$$\tilde{\theta}(0,t) = 0, \quad \tilde{\theta}(1,t) = -k_6\left(v_6 + \tilde{d}_6\right),$$
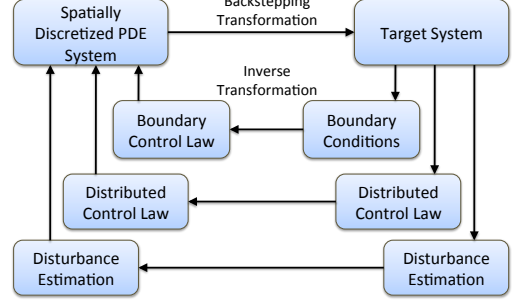

Fig. 2. Schematic of the backstepping control design.

where $\tilde{d}_k$ for $k = 1, \ldots, 6$ is the disturbance estimation error. Note that, while the proposed backstepping design can handle nonlinear terms, the term $\tilde{g}$ has been linearized in this case, i.e., we take $\tilde{g} \approx \hat{g}\tilde{\theta}$ where $\hat{g} = \frac{\partial \tilde{g}}{\partial \theta}\big|_{\theta=\theta_{ff}}$, to simplify the design and implementation of the controller in the DIII-D plasma control system (PCS), which is currently set up to handle linear controller systems coupled with nonlinear transformations, but not general nonlinear control laws. The objective of the controller is to force $\tilde{\theta}(\hat{\rho}, t)$ to zero using distributed actuators $v_k \ \forall k \in [1, 5]$, and the boundary actuator v_6, while accounting for the effect of disturbance estimation errors.

Figure 2 illustrates the control design approach. A backstepping technique is used to transform the original system into a particular target system. The target system is then rendered asymptotically stable through the choice of design parameters, boundary conditions, control laws for the distributed actuators, and update laws for the disturbance estimations. The combined boundary+interior control law is obtained using the inverse of the backstepping transformation.

Defining $h = \frac{1}{N}$, where N is an integer, and denoting $x^i(t) = x(ih, t)$, $i = 0, 1, \ldots, N$, the system is discretized as

$$\dot{\tilde{\theta}}^i = \left(h_{1a}^i\frac{\tilde{\theta}^{i+1} - 2\tilde{\theta}^i + \tilde{\theta}^{i-1}}{h^2} + h_{1b}^i\frac{\tilde{\theta}^{i+1} - \tilde{\theta}^{i-1}}{2h}\right.$$
$$\left. + h_{1c}^i\tilde{\theta}^i\right)u_{1_{ff}} + \left(h_{1a}^i\frac{\theta^{i+1} - 2\theta^i + \theta^{i-1}}{h^2}\right.$$
$$\left. + h_{1b}^i\frac{\theta^{i+1} - \theta^{i-1}}{2h} + h_{1c}^i\theta^i\right)\left(v_1 + \tilde{d}_1\right)$$
$$+ \sum_{k=2}^{4} h_k^i\left(v_k + \tilde{d}_k\right) + g^i\left(v_5 + \tilde{d}_5\right) + \hat{g}^i u_{5_{ff}}\tilde{\theta}^i, \tag{15}$$
$$\tilde{\theta}^0 = 0, \quad \tilde{\theta}^N = -k_6\left(v_6 + \tilde{d}_6\right). \tag{16}$$

The target system is chosen as

$$\dot{\tilde{w}}^i = \left(h_{1a}^i\frac{\tilde{w}^{i+1} - 2\tilde{w}^i + \tilde{w}^{i-1}}{h^2} + h_{1b}^i\frac{\tilde{w}^{i+1} - \tilde{w}^{i-1}}{2h}\right.$$
$$\left. + h_{1c}^i\tilde{w}^i - C_1\tilde{w}^i\right)u_{1_{ff}} + \hat{g}^i u_{5_{ff}}\tilde{w}^i + J^i\left(v_1 + \tilde{d}_1\right)$$
$$+ \sum_{k=2}^{4} H_k^i\left(v_k + \tilde{d}_k\right) + G^i\left(v_5 + \tilde{d}_5\right), \tag{17}$$
$$\tilde{w}^0 = 0, \quad \tilde{w}^N = -k_6\tilde{d}_6, \tag{18}$$

where C_1 is a design parameter and

$$J^i = \left(h_{1a}^i \frac{\theta^{i+1} - 2\theta^i + \theta^{i-1}}{h^2} + h_{1b}^i \frac{\theta^{i+1} - \theta^{i-1}}{2h} + h_{1c}^i \theta^i \right)$$
$$- \sum_{j=1}^{i-1} \frac{\partial \alpha^{i-1}}{\partial \tilde{\theta}^j} \left(h_{1a}^j \frac{\theta^{j+1} - 2\theta^j + \theta^{j-1}}{h^2} \right.$$
$$\left. + h_{1b}^j \frac{\theta^{j+1} - \theta^{j-1}}{2h} + h_{1c}^j \theta^j \right),$$
$$H_k^i = h_k^i - \sum_{j=1}^{i-1} \frac{\partial \alpha^{i-1}}{\partial \tilde{\theta}^j} h_k^j, \quad G^i = g^i - \sum_{j=1}^{i-1} \frac{\partial \alpha^{i-1}}{\partial \tilde{\theta}^j} g^j,$$

for $k = 2, 3, 4$. The term α is a backstepping transformation in the form $\tilde{w}^i = \tilde{\theta}^i - \alpha^{i-1}(\tilde{\theta}^0, \dots, \tilde{\theta}^{i-1})$. By subtracting (17) from (15), the expression $\dot{\alpha}^{i-1} = \dot{\tilde{\theta}}^i - \dot{\tilde{w}}^i$ is obtained in terms of $\alpha^{k-1} = \tilde{\theta}^k - \tilde{w}^k$, $k = i-1, i, i+1$. The resulting expression can be solved for α^i to yield

$$\alpha^i = \frac{1}{u_{1_{ff}}} \left(\frac{h_{1a}^i}{h^2} + \frac{h_{1b}^i}{2h} \right)^{-1} \left[- \left(h_{1a}^i \frac{-2\alpha^{i-1} + \alpha^{i-2}}{h^2} \right. \right.$$
$$- h_{1b}^i \frac{\alpha^{i-2}}{2h} + h_{1c}^i \alpha^{i-1} + C_1 \tilde{w}^i \Bigg) u_{1_{ff}} + \dot{\alpha}^{i-1}$$
$$- \left(h_{1a}^i \frac{\theta^{i+1} - 2\theta^i + \theta^{i-1}}{h^2} + h_{1b}^i \frac{\theta^{i+1} - \theta^{i-1}}{2h} \right.$$
$$+ h_{1c}^i \theta^i - J^i \Bigg)(v_1 + \tilde{d}_1) - \left(g^i - G^i \right)(v_5 + \tilde{d}_5)$$
$$\left. - \sum_{k=2}^4 \left(h_k^i - H_k^i \right)(v_k + \tilde{d}_k) - u_{5_{ff}} \hat{g}^i \alpha^{i-1} \right], \quad (19)$$

where $\alpha^0 = 0$ and $\dot{\alpha}^{i-1}$ is calculated as

$$\dot{\alpha}^{i-1} = \sum_{k=1}^{i-1} \left(\frac{\partial \alpha^{i-1}}{\partial \tilde{\theta}^k} \dot{\tilde{\theta}}^k + \frac{\partial \alpha^{i-1}}{\partial \theta_{ff}^k} \dot{\theta}_{ff}^k \right) + \sum_{j=1}^6 \frac{\partial \alpha^{i-1}}{\partial u_{j_{ff}}} \dot{u}_{j_{ff}}. \quad (20)$$

Through its dependence on $\dot{\tilde{\theta}}$, expression (20) depends on the to-be-designed distributed control laws which will not in general be spatially causal and would violate the strict-feedback structure required for backstepping. It also depends on the disturbance terms, which are unknown. However, by our choice of target system, the terms involving J^i, H_k^i, and G^i exactly remove the undesirable terms from the recursive expression (19), upon substitution, i.e.,

$$\alpha^i = \left(\frac{h_{1a}^i}{h^2} + \frac{h_{1b}^i}{2h} \right)^{-1} \left[- \left(h_{1a}^i \frac{-2\alpha^{i-1} + \alpha^{i-2}}{h^2} \right. \right.$$
$$\left. - h_{1b}^i \frac{\alpha^{i-2}}{2h} + h_{1c}^i \alpha^{i-1} + C_1 \tilde{\theta}^i - C_1 \alpha^{i-1} \right)$$
$$\left. - \frac{u_{5_{ff}}}{u_{1_{ff}}} \hat{g}^i \alpha^{i-1} + \frac{\dot{\alpha}_{strict}^{i-1}}{u_{1_{ff}}} \right], \quad (21)$$

where

$$\dot{\alpha}_{strict}^{i-1} = \sum_{k=1}^{i-1} \frac{\partial \alpha^{i-1}}{\partial \tilde{\theta}^k} \left[\left(h_{1a}^i \frac{\tilde{\theta}^{k+1} - 2\tilde{\theta}^k + \tilde{\theta}^{k-1}}{h^2} + h_{1c}^k \tilde{\theta}^k \right. \right.$$
$$\left. + h_{1b}^k \frac{\tilde{\theta}^{k+1} - \tilde{\theta}^{k-1}}{2h} \right) u_{1_{ff}} + \hat{g}^k u_{5_{ff}} \tilde{\theta}^k \Bigg]$$
$$+ \sum_{j=1}^6 \frac{\partial \alpha^{i-1}}{\partial u_{j_{ff}}} \dot{u}_{j_{ff}} + \sum_{k=1}^{i-1} \frac{\partial \alpha^{i-1}}{\partial \theta_{ff}^k} \dot{\theta}_{ff}^k. \quad (22)$$

Subtracting (18) from (16) and putting the resulting expression in terms of $\alpha^{k-1} = \tilde{\theta}^k - \tilde{w}^k$, $k = i-1, i, i+1$,

the control law for v_6 can be defined as

$$v_6 = -\frac{1}{k_6} \alpha^{N-1}. \quad (23)$$

Next, we design the control laws for the distributed actuators, as well as the update laws for the disturbance estimations to stabilize the target system. We consider the control Lyapunov function

$$V = \frac{1}{2} \sum_{i=1}^{N-1} Q_w^i \left(\tilde{w}^i \right)^2 + \frac{1}{2} \sum_{k=1}^6 \frac{\tilde{d}_k^2}{K_k},$$

where Q_w^i, for $i \in [1, N-1]$ are positive definite weights, and K_k are positive constants, and calculate

$$\dot{V} = -W^T A_W W u_{1_{ff}} + \sum_{k=1}^5 v_k \Theta_k + \sum_{k=1}^5 \tilde{d}_k \left[\Theta_k + \frac{\dot{\tilde{d}}_k}{K_k} \right]$$
$$+ \tilde{d}_6 \left[-k_{17} Q_w^{N-1} \tilde{w}^{N-1} \left[\frac{h_{1a}^{N-1}}{h^2} + \frac{h_{1b}^{N-1}}{h} \right] u_{1_{ff}} + \frac{\dot{\tilde{d}}_6}{K_6} \right], (24)$$

where A_W is positive definite, $W = [w^1, \dots, w^{N-1}]$, and

$$\Theta_1 = \sum_{i=1}^{N-1} Q_w^i \tilde{w}^i J^i, \quad \Theta_5 = \sum_{i=1}^{N-1} Q_w^i \tilde{w}^i G^i,$$
$$\Theta_k = \sum_{i=1}^{N-1} Q_w^i \tilde{w}^i H_k^i, \text{ for } k = 2, 3, 4,$$

are nonlinear, time-varying functions of the error measurements. We take the control laws and update laws

$$v_1 = -T_1 \Theta_1, \quad v_5 = -T_5 \Theta_5, \quad (25)$$
$$v_k = -T_k \Theta_k, \quad \forall k \in \{2, 3, 4\}, \quad (26)$$
$$\dot{\tilde{d}}_k = K_k \Theta_k, \quad \forall k \in \{1, \dots, 5\}, \quad (27)$$
$$\dot{\tilde{d}}_6 = -K_6 Q_w^{N-1} \tilde{w}^{N-1} \left[\frac{h_{1a}^{N-1}}{h^2} + \frac{h_{1b}^{N-1}}{h} \right] u_{1_{ff}}, \quad (28)$$

where $T_k \geq 0$ for $k = 1, 2, 3, 4, 5$, are design constants. Assuming constant disturbances, this reduces (24) to

$$\dot{V} = -W^T A_W W u_{1_{ff}} - \sum_{k=1}^5 T_k \Theta_k^2. \quad (29)$$

Since $\dot{V} \leq 0$, $V \geq 0$, and $\ddot{V}$ is bounded, the conditions of Barbalat's lemma (Khalil, 2002) are satisfied, and we have that $\dot{V} \to 0$. This implies that $\tilde{w}$ and consequently $\tilde{\theta}$ are driven to zero,. Note that the nonlinear control laws were linearized around the feedforward trajectories for implementation in the current version of the PCS.

The nonlinear transformations (12), must be inverted to obtain references for the physical actuators from the combined feedforward+feedback output of the controller. However, there is one more u variable than available physical actuators, meaning there is not, in general, a solution to the inverse transformation. To overcome this, an actuator that provides heating without driving current (to independently modulate P_{tot}), is required. On DIII-D, this additional degree of freedom could be achieved with a combination of co- and counter-current beam injection that drives very little current, however, counter-current beams were not used during the present experimental campaign. Instead, a weighted least squares fit was used to find the the individual beam and gyrotron powers that best fit the outputs of the controller.
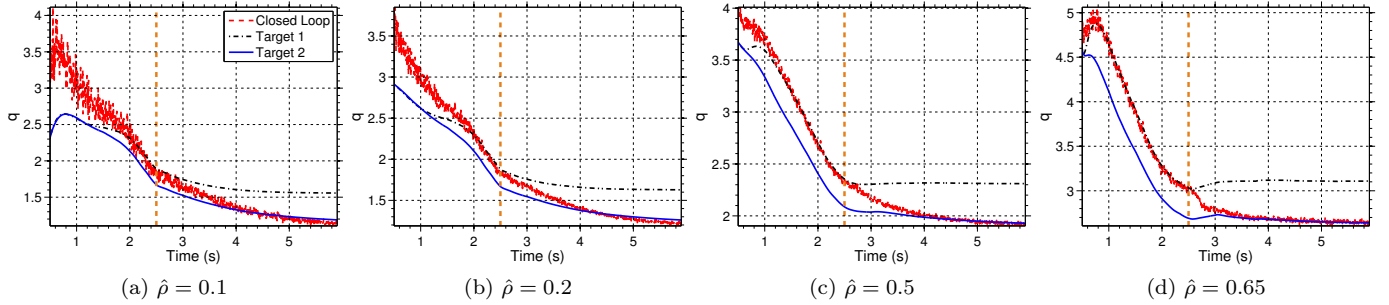
Fig. 3. Time traces of q comparing Targets 1 and 2 (black, dash-dot and blue, solid, respectively) with the closed loop simulation (red-dashed). The vertical orange dashed line shows when the controller target was switched.
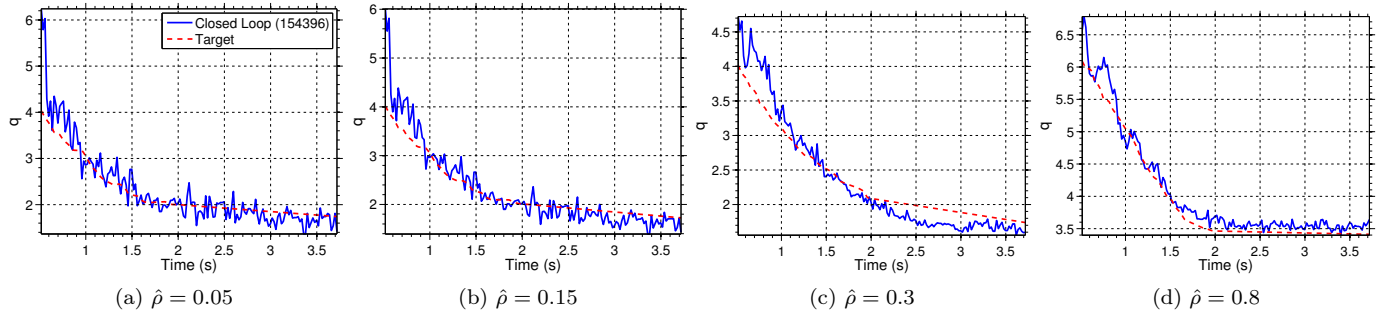
(a) $\hat{\rho} = 0.1$ (b) $\hat{\rho} = 0.2$ (c) $\hat{\rho} = 0.5$ (d) $\hat{\rho} = 0.65$

(a) $\hat{\rho} = 0.05$ (b) $\hat{\rho} = 0.15$ (c) $\hat{\rho} = 0.3$ (d) $\hat{\rho} = 0.8$

Fig. 4. Time traces of q comparing the closed loop (blue, solid) with the target (red-dashed) during shot #154398.

4. SIMULATION AND EXPERIMENTAL RESULTS

Prior to experimental testing, a simulation study was conducted in which the control-oriented model was simulated in closed loop. Based on physical considerations, the elements of Q were chosen to weight the points near $\hat{\rho} = 0$ and $\hat{\rho} = 1$ more heavily than the middle of the domain. The remaining design parameters were tuned to achieve desirable response time, disturbance rejection, and noise rejection, based on assumed disturbance and noise levels. As a test of target tracking capability, two input trajectories Feedforward 1 and Feedforward 2 were used to generate target current profile evolutions Target 1 and Target 2. In the closed loop simulation, Feedforward 1 was provided to the controller throughout the simulation. The initial conditions were perturbed, and the controller target was changed from Target 1 to Target 2 at 2.5s. Simulated noise was added to the measurements throughout the discharge. Time traces of q, shown in Figure 3, show that the controller was able to reject the initial condition errors (most noticeable in Figures 3a and 3b) and to achieve Target 1 prior to 2.5s. After the target was switched (indicated by the vertical orange dashed line) the controller was able to move the profile to Target 2 by 4.0s.

For the preliminary experimental test of the controller on DIII-D, a target profile was generated based on the results of an open loop reference shot #150320. Two of the beams were needed for the motional Stark Effect current profile diagnostic and were therefore unavailable for feedback. The feedforward trajectories for the remaining beams were modified from those used in the reference shot, acting as input disturbances. Furthermore, the gyrotrons, which were turned on at 2.5s in the reference shot, were unavailable during the closed loop shot. This reduced the available

current drive and heating, and contributed to increased MHD instabilities. The increased MHD activity caused the shot to terminate early at 3.7s. Time traces of q are presented in Figure 4, showing that, despite the disturbances and significant initial condition errors, the controller was able to achieve fairly good tracking of the desired target throughout the discharge. A drop in q near $\hat{\rho} = 0.3$ around $t = 2.5s$ is seen in Figure 4c, which corresponds to the time that gyrotrons were turned on in the reference shot. Figure 5 shows the q profile at various times, along with a shaded region representing the standard deviation of the measurements over a window of 0.25s prior to the displayed time. Initial errors, still visible at $t = 1.0s$ in Figure 5a, are mostly removed by $t = 1.5s$ (Figure 5b). After the previously mentioned drop in q at $t = 2.5s$, the desired profile is recovered by $t = 3.5s$ (Figures 5c and d). Figure 6 compares the achieved, requested (output of the controller), and feedforward actuator trajectories, showing the modification of the input trajectories by the controller. Density was reduced in response to the disturbances, while the plasma current began to oscillate around the desired reference (Figures 6a and b). This appears to have been a result of much higher than expected levels of noise, and may be addressed in future experiments by reducing the gain K_6. Because the lack of gyrotron power reduced the off-axis current drive, the controller responded by increasing the off-axis beam power (until it hit saturation) and decreasing the on-axis beam power (Figures 6c and d).

5. CONCLUSIONS

We have presented simulation and preliminary experimental results showing the performance of a backstepping boundary+interior current profile controller based on a first-principles-driven model of H-mode DIII-D discharges.
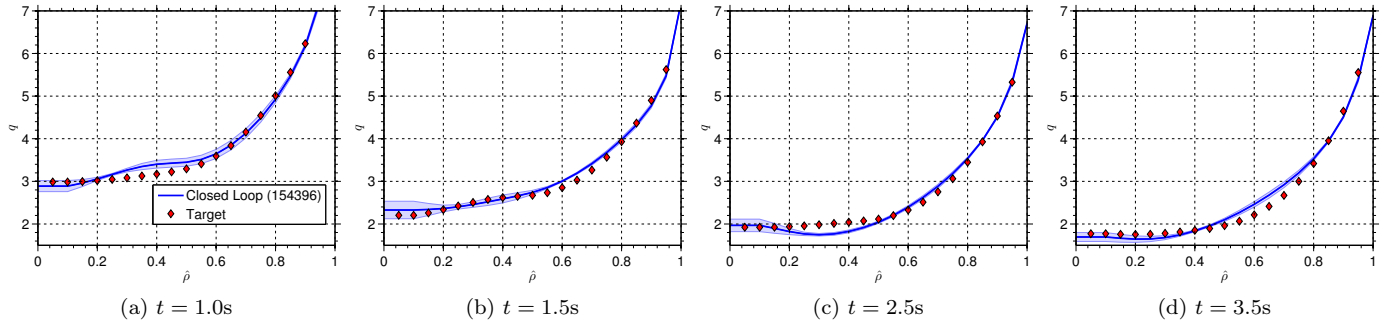
(a) $t = 1.0$s (b) $t = 1.5$s (c) $t = 2.5$s (d) $t = 3.5$s

Fig. 5. Profiles of q at various times during shot #154398 comparing closed loop profiles (blue solid) with the target (red diamonds). The shaded regions depict the standard deviation over a window of 0.25s prior to the time shown.

(a) Line-averaged density. (b) Plasma current. (c) Off-axis beam power. (d) On-axis beam power.
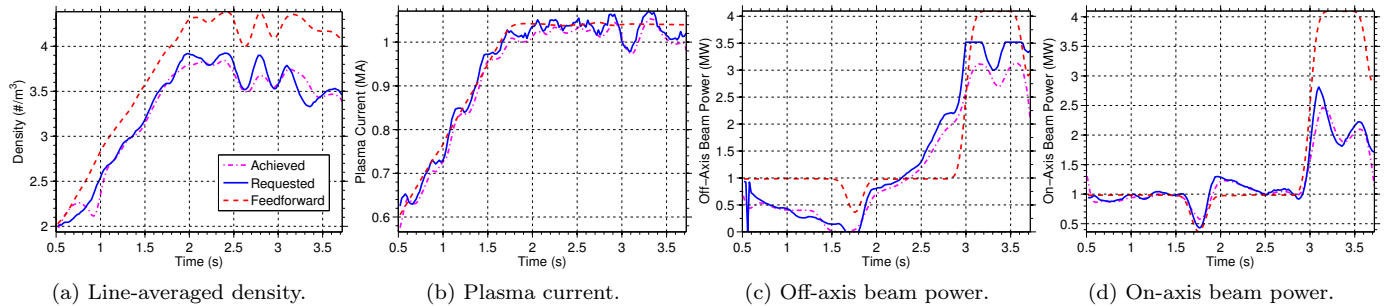
Fig. 6. Plots of density, plasma current, on-axis beam power, and off-axis beam power during shot #154398 comparing the feedforward values (red dashed) and the closed loop values (blue solid).

Further experimental testing, using gyrotron power and an implementation of the full nonlinear control laws, will be done to assess the controller in a variety of scenarios, including disturbance rejection and target tracking.

REFERENCES

Barana, O., Mazon, D., Laborde, L., and Turco, F. (2007). Feedback control of the lower hybrid power deposition profile on Tore Supra. *Plasma Physics and Controlled Fusion*, 49(7), 947–967.

Barton, J., Shi, W., and Schuster, E. (2013). Physics-Based Control-Oriented Modeling of the Safety Factor Profile Dynamics in High Performance Tokamak Plasmas. In *Proc. of the 52nd IEEE Conf. on Decision and Control*.

Barton, J., Boyer, M., Shi, W., Schuster, E., et al. (2012). Toroidal current profile control during low confinement mode plasma discharges in DIII-D via first-principles-driven model-based robust control synthesis. *Nuclear Fusion*, 52, 123018.

Boyer, M.D., Barton, J.E., Schuster, E., et al. (2014). Backstepping Control of the Toroidal Plasma Current Profile in the DIII-D Tokamak. *IEEE Transactions on Control Systems Technology*, (in press).

Boyer, M.D., Barton, J., Schuster, E., et al. (2013). First-principles-driven model-based current profile control for the DIII-D tokamak via LQI optimal control. *Plasma Physics and Controlled Fusion*, 55(10), 105007.

Ferron, J., Gohil, P., Greenfield, C., et al. (2006). Feedback control of the safety factor profile evolution during formation of an advanced tokamak discharge. *Nuclear Fusion*, 46(10), L13–L17.

Hinton, F.L. and Hazeltine, R.D. (1976). Theory of plasma transport in toroidal confinement. *Rev. of Modern Physics*, 48, 239.

Khalil, H.K. (2002). *Nonlinear Systems*. Prentice Hall, 3rd edition.

Laborde, L., Mazon, D., Moreau, D., et al. (2005). A model-based technique for integrated real-time profile control in the JET tokamak. *Plasma Physics and Controlled Fusion*, 47(1), 155–183.

Moreau, D., Mazon, D., Ariola, M., , et al. (2008). A two-time-scale dynamic-model approach for magnetic and kinetic profile control in advanced tokamak scenarios on JET. *Nuclear Fusion*, 48(10), 106001.

Murakami, M., Wade, M.R., Greenfield, C.M., et al. (2006). Progress toward fully noninductive, high beta conditions in DIII-D. *Physics of Plasmas*, 13(5), 056106.

Ou, Y., Luce, T., Schuster, E., et al. (2007). Towards model-based current profile control at DIII-D. *Fusion Engineering and Design*, 82(5-14), 1153–1160.

Ou, Y., Xu, C., Schuster, E., et al. (2008). Design and simulation of extremum-seeking open-loop optimal control of current profile in the DIII-D tokamak. *Plasma Physics and Controlled Fusion*, 50(11), 115001.

Sauter, O., Angioni, C., and Lin-Liu, Y.R. (1999). Neo-classical conductivity and bootstrap current formulas for general axisymmetric equilibria and arbitrary collisionality regime. *Physics of Plasmas*, 6(7), 2834.

Suzuki, T., Ide, S., Oikawa, T., et al. (2008). Off-axis current drive and real-time control of current profile in JT-60U. *Nuclear Fusion*, 48(4), 045002.

Wijnands, T., Houtte, D.V., Martin, G., et al. (1997). Feedback control of the current profile on Tore Supra. *Nuclear Fusion*, 37(6), 777–791.

Xu, C., Ou, Y., Dalessio, J., Schuster, E., et al. (2010). Ramp-up-phase current-profile control of tokamak plasmas via nonlinear programming. *IEEE Trans. on Plasma Sci.*, 38(2), 163–173.